

# Detecting and Monitoring Bias for Subgroups in Breast Cancer Detection AI

Amit Kumar Kundu<sup>1,5\*</sup>, Florence X. Doo<sup>3</sup>, Vaishnavi Patil<sup>4,5</sup>,  
Amitabh Varshney<sup>4,5,6</sup>, Joseph Jaja<sup>1,5,6</sup>

<sup>1\*</sup>Department of Electrical and Computer Engineering, University of Maryland.

<sup>3</sup>Department of Diagnostic Radiology and Nuclear Medicine, University of Maryland School of Medicine.

<sup>4</sup>Department of Computer Science, University of Maryland.

<sup>5</sup>Institute for Health Computing, University of Maryland.

<sup>6</sup>University of Maryland Institute for Advanced Computer Studies.

\*Corresponding author(s). E-mail(s): [amit314@umd.edu](mailto:amit314@umd.edu);  
Contributing authors: [FDoo@som.umaryland.edu](mailto:FDoo@som.umaryland.edu); [vspatil@umd.edu](mailto:vspatil@umd.edu);  
[varshney@umd.edu](mailto:varshney@umd.edu); [josephj@umd.edu](mailto:josephj@umd.edu);

## Abstract

Automated mammography screening plays an important role in early breast cancer detection. However, current machine learning models, developed on some training datasets, may exhibit performance degradation and bias when deployed in real-world settings. In this paper, we analyze the performance of high-performing AI models on two mammography datasets—the Emory Breast Imaging Dataset (EMBED) and the RSNA 2022 challenge dataset. Specifically, we evaluate how these models perform across different subgroups, defined by six attributes, to detect potential biases using a range of classification metrics. Our analysis identifies certain subgroups that demonstrate notable underperformance, highlighting the need for ongoing monitoring of these subgroups’ performance. To address this, we adopt a monitoring method designed to detect performance drifts over time. Upon identifying a drift, this method issues an alert, which can enable timely interventions. This approach not only provides a tool for tracking the performance but also helps ensure that AI models continue to perform effectively across diverse populations.

**Keywords:** Breast cancer detection, Mammography, AI model, Comprehensive Analysis

# 1 Introduction

Early breast cancer detection (BCD) through mammography screening continues to be a major focus in radiology as it plays a critical role in reducing mortality rates (Coleman (2017); Ginsburg et al. (2020)). Although artificial intelligence (AI) models can help radiologists to evaluate mammograms (Sahu et al. (2023); Evans et al. (2013); Maxwell (1999)), training such models face the challenge of limited datasets that may not fully represent all subgroups or cover variations in data distributions.

Historically, certain racial groups face barriers to healthcare access because of many socio-economic factors (Azin et al. (2023); Hershman et al. (2005); Hussain-Gambles et al. (2004)). This lack of access can result in datasets that do not adequately represent these groups, potentially cause AI models to show biases for these groups. Even with seemingly balanced datasets, subtle biases may persist in the collected data due to systemic inequalities in the quality of healthcare (Obermeyer et al. (2019)). Among these groups, African American patients are often underrepresented in both breast imaging and broader healthcare datasets (Yedjou et al. (2019); Newman and Kaljee (2017)). Moreover, studies show that models trained with well optimized design choices on a limited dataset performs well on data similar to the training distribution but struggle when tested on different demographics or varying imaging characteristics (De Vries et al. (2019); Wilson et al. (2019)). This raises concerns about the performance of such AI models across different demographic and other sensitive attributes in real-world clinical practice.

Several studies investigated the impact of potential biases on the performance of AI models across different demographic and clinical subgroups (Sun et al. (2022); Afzal et al. (2023); Mehta et al. (2024)). Addressing these biases through a comprehensive analysis of these models can help developers build more reliable systems that can be refined over time to improve healthcare outcomes for all patients. The development of such a framework necessitates large datasets that cover diverse demographics with relevant clinical information. Recently, Nguyen et al. (2024) analyzed the performance of a commercially available model exclusively on negative Digital Breast Tomosynthesis (DBT) examinations across different demographic groups. While the study highlights discrepancies in false positive rates among certain subgroups, it does not address the characteristics of the model’s training data, leaving questions about potential sources of bias unanswered.

Moreover, during clinical deployment, BCD-AI models are likely to encounter data distributions that differ from their training data due to shifts in subgroup composition, updates in scanning technology, and site-specific variations in imaging protocols and clinical workflows. This may result in a reduced or biased model performance, which can lead to missed diagnoses or delayed treatments. Therefore, an appropriate performance monitoring method is of high significance to quickly detect performance degradations and to ensure clinically actionable insights necessary for follow up adjustments.

This paper investigates the reliability of high-performing AI models in BCD by analyzing their performance across different demographic and clinical subgroups. To achieve this, we leverage two large and diverse datasets—the RSNA Screening Mammography Breast Cancer Detection dataset (Carr et al. (2022)) and the EMory BrEast

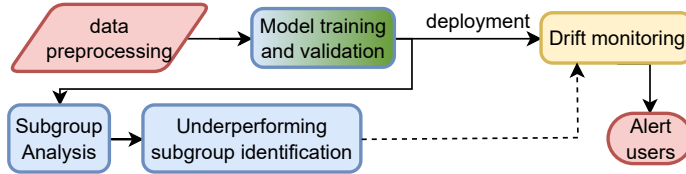


**Fig. 1:** Overview of the proposed framework. The framework assesses BCD performance across subgroups to understand the impacts of different attributes, enabling pre-deployment bias identification and post-deployment drift monitoring for alerts.

Imaging (EMBED) dataset (Jeong et al. (2023))—which contain extensive patient information. This comprehensive analysis provides a unique opportunity to assess potential biases in AI models and gain deeper insights into the characteristics of these datasets (Sweeney et al. (2022)).

We begin by analyzing the performance of high-performing AI models on the RSNA and EMBED datasets, focusing on identifying and evaluating performance across demographic and clinical subgroups. To explore these biases, we develop our own EMBED-AI model, which achieves strong results across multiple performance metrics. Despite its overall high performance, we demonstrate that biases in the dataset can lead to disparities in clinical outcomes for certain subgroups. To address this, we implement a performance monitoring method based on statistical process control (SPC) from Zamzmi et al. (2024); Prathapan et al. (2024); Feng et al. (2022), enabling the detection of model performance degradations over time. Fig. 1 provides an overview of the proposed framework. By systematically identifying disparities through subgroup analysis and tracking their performance over time, this framework allows for ongoing refinement of the model to ensure both reliability and fairness for all patients.

The main contributions of the paper can be summarized as follows:

- We train a new AI model on the large EMBED dataset using advanced computer vision techniques, such as strong data augmentations, cosine annealing, label smoothing, dropout with drop-path regularization, the exponential moving averaging of model weights and training with a significant model architecture while optimizing performance within limited computational resources. The model achieves excellent results across multiple performance metrics, including Positive Predictive Value (PPV), sensitivity, F1-score, and Area Under the Receiver Operating Characteristic Curve (AUROC).
- We conduct a rigorous performance analysis across subgroups in the RSNA dataset using its top-performing model and in the EMBED dataset using our trained model. The subgroups are defined based on key attributes, including age, race, breast tissue density, mammogram scanning technology, view position, and clinical site. Through this analysis, we identify subgroups for which each model exhibits bias and discuss their clinical implications.
- We adopt Statistical Process Control (SPC) methods, such as the cumulative sum (CUSUM) control chart, as a performance monitoring approach to enable continuous tracking and detection of performance drifts. This method can enable practitioners

to systematically assess model stability over time. Our findings demonstrate that CUSUM can effectively and rapidly identify performance drifts in underperforming subgroups.

The remainder of the paper is structured as follows: Section 2 introduces the datasets, evaluation protocols, and experimental setup. In Section 3, we present the overall performance of each model, followed by the results of the subgroup analysis and an evaluation of the performance monitoring method. Finally, Section 5 provides concluding remarks.

## 2 Materials and Methods

In this section, we present the datasets, the corresponding AI models, and the evaluation metrics used in our analysis. We also describe the method for monitoring performance.

### 2.1 Detection Task

We frame the AI task as a binary classification problem from a mammogram. The model for the RSNA dataset (Carr et al. (2022)) is trained on the defined *Cancer* variable as target. For EMBED, we define the target using the well-established Breast Imaging Reporting and Data System (BIRADS) scores of the mammograms (Sickles (2013)). Physicians assign BIRADS scores (from 0 to 6) to the mammograms in a standard way as described in Table A2 in Appendix A. We combine the benign and normal findings (BIRADS scores of 1 and 2) to construct the *Negative* class, and the suspicious through the malignancy findings (BIRADS scores of 4, 5 and 6) to create the *Positive* class. We categorize mammograms labeled as suspicious or highly suspicious under the *Positive* class, as these cases typically require further evaluation through biopsy to determine the final diagnosis. Mammograms with BIRADS 0 are excluded from the classification task, as these mammograms necessitate follow-up diagnostic imaging; however, we include the follow up diagnostic images in the dataset.

### 2.2 Datasets

The datasets commonly used to train BCD-AI models often lack sufficient mammograms, especially positive cases (Khaled et al. (2021); Cui et al. (2021); Pham et al. (2022); Lekamlage et al. (2020); Heath et al. (1998)), making them unsuitable for comprehensive analysis.

To address this limitation, the Radiological Society of North America (RSNA) hosted in 2022 a challenge using a dataset of 54,706 screening mammograms with a prevalence<sup>1</sup> of 2.12% to facilitate the training of BCD-AI models (Carr et al. (2022)). While the dataset includes important attributes such as tissue density, view position, and age, it lacks diagnostic mammograms and does not provide racial or ethnic descriptions of the participants. The details of the dataset for different attributes are

---

<sup>1</sup>Prevalence is defined as the ratio of positive samples to the total number of samples in a dataset.

outlined in Table 1. The absence of racial information may limit the dataset’s representation across all racial groups, potentially excluding those with a higher prevalence of breast cancer.

Recently, Emory University School of Medicine released the EMBED mammography dataset, which is large, granular and covers racially diverse demographics (Jeong et al. (2023)). The publicly available portion contains a large number of screening and diagnostic mammograms from a large number of patients. The dataset provides information related to different relevant attributes with pathological reports where appropriate. We only consider 2D mammograms with MLO and CC view positions resulting in a set of 217672 mammograms from 20128 participants and 56480 examinations. Mammogram examples are presented in Fig. A1 and the distributions of these attributes are provided in Table 1. We discuss the attribute distributions along with the performance analysis in details in Section 3.2. Moreover, to understand the inter-relationship between the considered attributes within dataset, the statistical associations between attributes for both datasets are presented later in Table B3.

Table 1 indicates that both EMBED and RSNA are highly imbalanced datasets with a prevalence of 3.37% and 2.12%, respectively. Moreover, considering the number of samples and prevalence of subgroups, the RSNA dataset distribution differs significantly from EMBED.

### 2.3 Training Method

We focus on the top-performing BCD-AI model developed by Nguyen (2023) for the RSNA 2022 challenge (Carr et al. (2022)). This model is built on a lightweight ConvNeXt backbone architecture (Liu et al. (2022)) and is trained on both the challenge dataset and additional external mammography datasets, such as VinDr-Mammo, MiniDDSM, CMMD, BMCD and CDD-CESM datasets (see Section 4). ConvNeXt, a high-capacity convolutional neural network, is designed to offer competitive performance with Vision Transformers and Swin Transformers while maintaining lower computational complexity, making it well-suited for large-scale computer vision tasks.

For EMBED dataset, we train our model using strong data augmentations (Appendix B.2), cosine annealed learning rate scheduling (Loshchilov and Hutter (2016)), label smoothing for positive samples (Lukasik et al. (2020)), dropout with drop-path regularization (Huang et al. (2016)), the exponential moving averaging of model weights (Morales-Brotons et al. (2024)) and training with the ConvNext model (Liu et al. (2022)). To efficiently train the model within the available computational resources (four A5000 GPUs), we use the pretrained model by Nguyen (2023) and apply transfer learning to achieve a significant performance improvement. In particular, we freeze the lower layers of the pretrained model, which are effective at learning low-level features relevant to mammography, allowing them to serve as rich mammogram feature extractors. We then train only the final stage and the head of the model, resulting in 15 million trainable parameters out of a total of 50 million. Training the model on such a diverse dataset with advanced training techniques makes our model suitable for the comprehensive analysis. The model outputs a probability of a positive prediction through a single output node with sigmoid activation. To address data imbalance, we employ a balanced batch sampler, maintaining a 1:1 ratio of positive

**Table 1:** Distribution of BIRADS scores and attributes in the filtered EMBED and the RSNA Datasets.

	EMBED			RSNA		
	(+) ves	(-) ves	prevalence (%)	(+) ves	(-) ves	prevalence (%)
Whole set	7346	210326	3.37	1158	53548	2.12
BIRADS Score						
0				664	7585	8.05
1		192351			15772	-
2		17975			2265	-
4	6263					
5	368					
6	715					
Subgroup						
Age Group						
age < 40	936	2390	28.14	5	471	1.05
40 ≤ age < 50	1848	44428	3.99	90	9958	0.90
50 ≤ age < 60	1693	57850	2.84	281	18383	1.51
60 ≤ age < 70	1519	59687	2.48	418	17585	2.32
40 ≤ age < 80	874	36483	2.34	306	6042	4.82
age ≥ 80	476	9488	4.78	58	1109	4.97
Race				Site		
Caucasian	2822	92462	2.96	1   664	28855	2.25
AAB	3693	92390	3.84	2   494	24693	1.96
Asian	345	11163	3.00			
AIAN	19	365	4.95			
NHPI	67	1604	4.01			
Multiple	14	551	2.48			
Unknown	386	11791	3.17			
Tissue density						
1	558	26335	2.07	53	3052	1.71
2	2460	91133	2.63	309	12342	2.44
3	3521	82025	4.12	277	11898	2.28
4	598	10307	5.48	25	1514	1.62
View position						
MLO	3145	112528	2.72	590	27313	2.11
CC	4201	97798	4.12	566	26199	2.11
Scanner				Machine ID for RSNA		
Lorad Selenia	176	7197	2.39	021   154	8067	1.87
Selenia Dimensions	6680	185708	3.47	029   161	8106	1.95
S2000D ADS17.4.5	237	7634	3.01	048   179	8520	2.06
S2000D ADS17.5	34	1094	3.01	049   614	22915	2.61
S Ess. ADS53.40	197	8313	2.31	093   14	1901	0.73
S Pristina	19	380	4.76	170   23	900	2.49
(S for Senograph)				190   05	140	3.45

to negative samples. Further augmentation, training and preprocessing details of each mammogram to extract  $1024 \times 2048$  region of interest (ROI) input are described in Appendix B. A four-fold cross validation is performed. We observe similar BIRADS distributions and subgroup distributions for each attribute across the folds even though we do not consider any attribute information for data splitting.

## 2.4 CUSUM-based Performance Monitoring

CUSUM control chart is a powerful tool to continuously monitor and control the quality of a statistical process (Crosier (1986)). This tool can be used to drift in data characteristics or detect degradation in model performance over time as demonstrated in Prathapan et al. (2024); Zamzmi et al. (2024). In this work, we employ a CUSUM-based method to monitor performance drift in under-represented or under-performing subgroups. This approach helps flag potential biases in model performance and prevent unfair evaluations.

We track drift in a specific performance metric, such as sensitivity of the model, which is assessed at the batch level. Initially, our model processes batches that closely resemble the data distribution seen during training. Over time, it encounters shifted distributions that may lead to performance degradation. To evaluate our monitoring method, we create a simulated scenario with  $N$  batches as a sequential data. The batches comprise of  $B$  mammograms with bootstrapped sampling. For simulating the monitoring of performance degradation due to changes in data distribution of one attribute (say, age), we first empirically compute the base marginal distribution  $p_{base} = [p_0, p_1, \dots, p_l]$  for the attribute from the overall training data, where  $p_l$  is the proportion of  $l$ -th subgroup in the training data.

We assume that the first  $N/2$  batches are constructed from  $p_{base}$  with a small flexibility (say,  $\pm 2.5\%$ ) around the base proportions. Starting halfway through the process, we start introducing deviations in attribute distribution by removing or adding more samples from a certain subgroup  $u$  to each batch at a portion  $p'_u = p_u + \Delta p$ .  $u$  is selected from the subgroups and  $\Delta p$  is varied within a range. This simulation is designed to detect when the metric scores are below the acceptable range with CUSUM charts by varying the deviations of data distribution in amount and direction.

The CUSUM control signals  $S_i^u$  and  $S_i^l$ , to detect an upward or a downward shift, are computed as:

$$\begin{aligned} S_i^u &= \max(0, S_{i-1}^u + (m_i - \mu - k)) \\ S_i^l &= \min(0, S_{i-1}^l + (m_i - \mu + k)) \end{aligned}$$

where  $m_i$  is the computed metric for  $i$ -th batch,  $\mu$  is the mean value of the metric, and  $k$  is an allowance. A drift is detected when one of the control signals is outside the threshold range  $(-h, h)$ .  $h = 4\sigma$ , where  $\sigma$  is the standard deviation of the metric. Prior to deployment, we only need to calculate the mean  $\mu$  and standard deviation  $\sigma$ , which are derived from the training batches. The sensitivity of the CUSUM control chart is fine-tuned by adjusting the parameters  $k$  and  $h$ , which strikes a balance between false alarm and delays in drift detection.

## 2.5 Evaluation Metrics

We used three set of metrics: classification metrics, statistical significance metrics, and monitoring metrics as described next.

The performance of the models are evaluated using positive predictive value (PPV or precision), sensitivity (or recall), F1 score, accuracy, specificity, area under the

**Table 2:** Performance [average(standard deviation)] on the overall datasets for their respective targets

Model	dataset	PPV	sensitivity	F1 score	AUROC
Nguyen (2023)	RSNA	0.548(0.099)	0.500(0.07)	0.523(0.08)	0.916(0.035)
This work	EMBED	0.896(0.01)	0.679(0.014)	0.773(0.006)	0.945(0.001)

receiver operating characteristic curve (AUROC), and Monte Carlo (MC) dropout uncertainty. Sensitivity is important due to the low true positive detection rates in breast cancer diagnosis and PPV is important because of low success rates in positive predictions. To select the best detection threshold, we search for the highest training F1 score within the threshold range of  $\{0.01, 0.02, \dots, 1.0\}$  and compute all metrics using the fixed threshold during testing. Selecting the threshold based on the highest F1 score creates a balance between PPV and sensitivity for such an imbalanced dataset scenario.

For attributes divided into exactly two subgroups, we use the Mann-Whitney U test (Mann and Whitney (1947)) to measure the statistical significance of differences in performance between these subgroups. For attributes categorized into more than two subgroups, we use the Kruskal-Wallis test (Kruskal and Wallis (1952)) to determine if significant differences exist among the groups. If significant, we then conduct Dunn’s posthoc analysis (Dunn (1964)) for detailed pairwise comparisons. To assess correlations between two continuous variables, we apply Pearson’s correlation test and to assess associations between two categorical variables, we perform the Cramer’s V association test. The significance level is set at 0.05 for all analyses.

We assessed the performance of CUSUM in detecting drift using two key metrics: the False Alarm Rate (FAR) and Detection Delay. FAR measures how frequently the method incorrectly signals a change when there is no actual drift. A low FAR is desirable as it indicates that the method minimizes unnecessary alerts, thus avoiding the costs and disruptions of false positives. Detection Delay, on the other hand, measures the time or the number of data points required for the method to identify a true change once it has occurred. Minimizing detection delay ensures that any significant changes are recognized promptly, allowing for quick response to actual drift.

### 3 Results and Discussions

We present three sets of results. The first set shows the performance of the models on the overall datasets. We then show the results of analyzing the models’ consistency across subgroups. Finally, we demonstrate the effectiveness of applying CUSUM to detect drift in the models’ performance.

#### 3.1 Model Performance

Before conducting subgroup analysis, it is important to ensure the models achieve acceptable performance on the respective datasets. Therefore, we evaluate the performance of the model developed by Nguyen (2023) on the RSNA dataset and our trained model (described in Section 2.3) on the EMBED dataset, with the results presented in Table 2. We observe that the model by Nguyen (2023) achieves an AUROC of 91.6% on

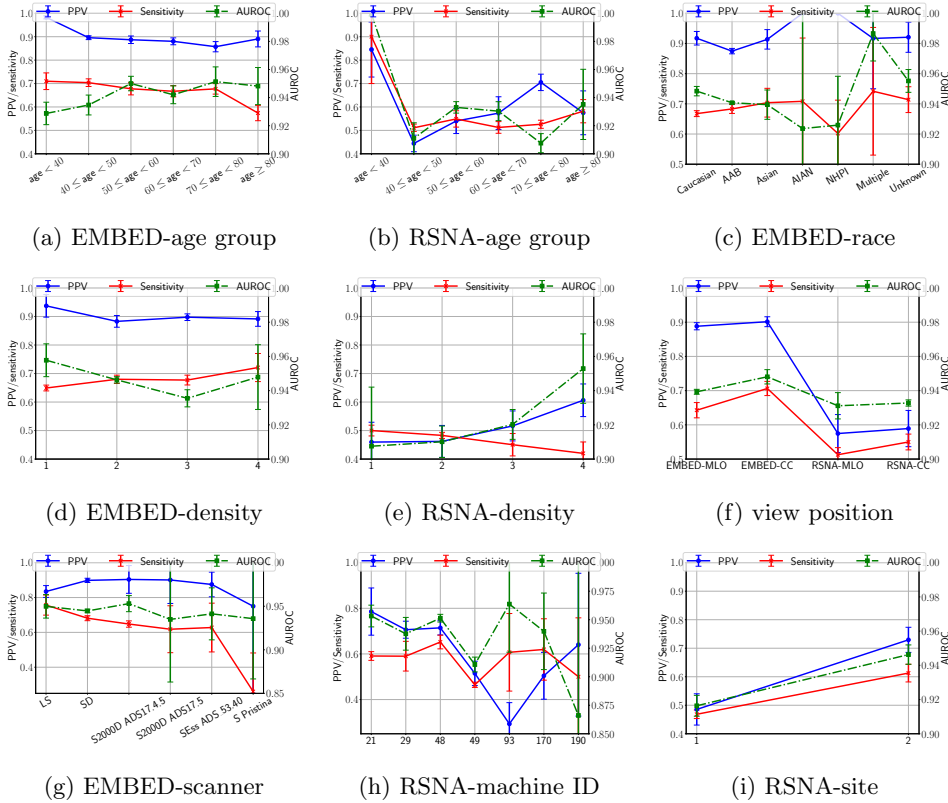


**Fig. 2:** Model performance for different attributes. PPV and sensitivity are shown on the left axis, while AUROC is shown on the right axis. Error bars represent the standard deviation of metrics.

RSNA. The Table also shows that our model achieves good performance on EMBED across different metrics. Moreover, our model outputs significantly higher probability scores for the positive cases than the negative cases (median: 0.80 [interquartile range (IQR): 0.56–0.81] vs median: 0.05 [IQR: 0.02–0.13],  $p \approx 0.0$  from Wilcoxon rank-sum test). The overall AUROC of our model is 0.9448. Considering the small prevalence, PPV and sensitivity are more important for positive detections.

### 3.2 Subgroup Analysis

We utilize the pretrained model and our trained model to perform subgroup analysis on RSNA and EMBED, respectively. We discuss model performance in relation to the data distribution across subgroups defined by the following attributes: age; race; breast tissue density; view positions; site; and scanning technology. We present our results using the metrics: PPV, sensitivity and AUROC and list all the metrics in Appendix C.1: Table C4 and Table C5. The objective of this analysis is to determine if there are

performance disparities affecting specific subgroups, even within models that generally perform well, and to explore the implications of these disparities. For all attributes, we reference Table 1 to examine the distribution of subgroups in our discussion.

### 3.2.1 Age

Results for different age groups are shown in Figs. 2a and 2b. For EMBED, participants of age  $< 40$  has a high prevalence of 28.14%. After this, the prevalence gradually decreases from 4% to 2.34% with increasing age range except for the group with age  $\geq 80$  when it goes up to 4.78%. One potential explanation for the high prevalence of participants of age  $< 40$  is the selection bias - for instance, oversampling of high-risk younger patients, rather than routine screening cohorts. This skew may inflate the model’s apparent performance in younger patients and may not reflect a typical population distribution.

We observe that sensitivity declines with increasing age group (coefficient,  $\rho = -0.8380, p < 0.04$ ). In particular, we observe a significant drop in sensitivity for the group with age  $\geq 80$  than age  $< 50$  ( $p = 0.02$ ). To be specific, the Caucasian population with age  $\geq 80$  has a lower sensitivity (51.27%) despite the fact that the overall sensitivity of Caucasian population is not impacted by this drop (see Section 3.2.2). While subgroup-specific threshold recalibration for this age group increased sensitivity by 4.71% with a minor drop in specificity (by 0.41%), this improvement remained well-below the overall average sensitivity. It is to be noted that the U.S. Preventive Services Task Force recommends routine screening from 40 to 74 years of age (Nicholson et al. (2024)), so our observed performance decline in patients for age  $\geq 80$  raises questions about the model’s generalizability beyond recommended screening intervals. Future work could explore specialized or alternative imaging strategies for this age group. Higher PPV is achieved for the group with age  $< 40$  than the ‘ $70 \leq \text{age} < 80$ ’ subgroup ( $p < 0.004$ ). A significant correlation is found between the prevalence and the PPV ( $\rho = 0.9668, p < 0.002$ ) for the age groups. AUROC is lower for the ‘age  $< 40$ ’ subgroup than the ‘ $70 \leq \text{age} < 80$ ’ subgroup and it increases with increasing age group (coefficient,  $\rho = 0.8145, p < 0.05$ ).

For RSNA, prevalence increases with increasing age group from 0.90% to 4.97%. Sensitivity is higher for the ‘age  $< 40$ ’ group than the ‘ $40 \leq \text{age} < 50$ ’ ( $p = 0.02$ ) and ‘ $60 \leq \text{age} < 70$ ’ ( $p = 0.04$ ) subgroups. However, there are only a few number of positive cases for age  $< 40$ . PPV is lower for the ‘ $40 \leq \text{age} < 50$ ’ group than the ‘age  $< 40$ ’ ( $p = 0.002$ ) and ‘ $70 \leq \text{age} < 80$ ’ ( $p = 0.04$ ) subgroups. Moreover, AUROC is lower for the ‘ $40 \leq \text{age} < 50$ ’ ( $p < 0.02$ ) and ‘ $70 \leq \text{age} < 80$ ’ ( $p = 0.003$ ) subgroups than the ‘age  $< 40$ ’ group.

### 3.2.2 Race

Table 1 and Fig. 2c present the distribution and performance based on different racial groups in EMBED. No racial information is found for RSNA. A higher prevalence is found for the African American or Black (AAB) (3.84%), Native Hawaiian and Pacific Islanders (NHPI) (4.01%), and American Indian and Alaskan Native (AIAN) (4.95%) groups than the overall prevalence. The model scored a lower PPV for the AAB population ( $p < 0.007$ ). Here, most mammograms of AAB population are from

the Selenia Dimensions scanner (Section 3.2.5) with a PPV of 87.29%. Similarly, a drop in sensitivity is observed for the NHPI group though it does not appear to be significant in the test. The high variability in sensitivity with only few positive samples for the AIAN, NHPI, and Multiple groups indicate that the sensitivity estimates might be unreliable for these groups. No significant difference is found among the AUROC scores of racial groups ( $p > 0.05$ ).

### 3.2.3 Tissue Density

The subgroup distribution and the evaluation metrics based on breast tissue density are presented in Table 1, and Figs. 2d and 2e. The definitions of tissue densities are presented in Table A1 in Appendix A. We ignore the male tissue density (density of 5). For EMBED, we observe that prevalence increases with tissue density ( $\rho = 0.9955, p \approx 0.05$ ), especially a high prevalence (5.48%) is found for density of 4. Sensitivity is higher for the density of 4 than density of 1 ( $p < 0.02$ ). Specifically, AAB population with tissue density of 1 has a lower sensitivity (62.05%) though it is not reflected in the overall AAB sensitivity score. No significant difference is found among the PPV and AUROC scores ( $p > 0.05$ ).

For RSNA, the model achieves higher AUROC for density of 4 than density of 2 ( $p < 0.03$ ). No significant difference is found among the PPV scores. Sensitivity decreases with the tissue density ( $\rho = -0.9919, p = 0.008$ ). The observed lower sensitivity for RSNA in denser breast categories (BIRADS C or D) aligns with clinical experience, where extremely dense breast tissue can mask malignancies. Consequently, patients with higher densities may benefit from alternative or supplemental screening (e.g., ultrasound, MRI, or DBT). However, similar results may not be expected from the EMBED model as the target variable is different.

### 3.2.4 View Position

The distribution and performance metrics based on MLO and CC view positions are shown in Table 1, Fig. 2f. For EMBED, even though the model achieves similar PPV for both view positions ( $p = 0.3429 > 0.05$ ), there is a significant drop in sensitivity by 6.35% and in AUROC by 0.88% ( $p < 0.03$ ) for the MLO view position. MLO projection is clinically important for visualizing the upper-outer breast. Even a modest performance drop in MLO views might risk overlooking certain lesions. Follow-up analysis should evaluate if the model captures morphological cues equally across both MLO and CC, or whether additional MLO-specific training data might be warranted. However, no significant difference is found in performance between the views for the RSNA dataset.

### 3.2.5 Scanning Technology

The distribution and the performance metrics based on different scanners are presented in Table 1, and Figs. 2g and 2h. We observe that for EMBED, most of the samples are from Selenia Dimensions. No significant difference is found in the evaluation metrics among the different machines except that Senograph (S) Pristina achieves a significantly lower average sensitivity ( $p < 0.007$ ). This might happen due the low

**Table 3:** Association ( $p < 0.05$ ) of variables with target and predicted label

	EMBED					
group	age group	race	tissue density	view position	machine ID	
target	<b>0.1754</b>	0.0242	<b>0.0527</b>		0.0387	0.0262
Predicted label	<b>0.1441</b>	0.0256	<b>0.0487</b>		0.0398	0.027
	RSNA					
group	age group	site	tissue density	view position	machine ID	
target	<b>0.0836</b>	0.0099	0.0175	< 0.0001 <sup>2</sup>		0.043
Predicted label	<b>0.0637</b>	0.0255	0.0274	0.0012 <sup>2</sup>		0.035

<sup>2</sup>indicates that the association is not significant ( $p > 0.05$ )

number of samples from this scanner. However, we observed a negative correlation between prevalence and sensitivity scores ( $\rho = -0.867, p < 0.03$ ).

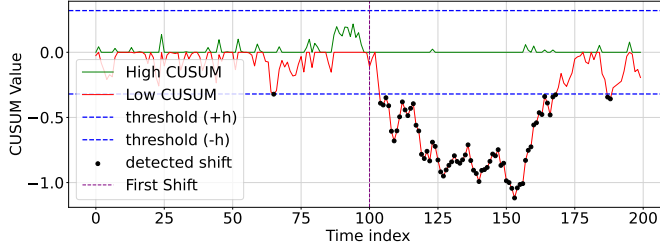
In RSNA, instead of scanner names, machine IDs are provided, where machines 21, 29 and 48 are present at site 2 and the rest are present at site 1. Almost 45% samples are from machine 49. Similar to EMBED, no significant difference is found in evaluation metrics among the different machines in the RSNA dataset except that machine 93 achieves a significantly lower average PPV ( $p < 0.02$ ). However, we observe a negative correlation between prevalence and AUROC scores ( $\rho = -0.867, p < 0.01$ ).

### 3.2.6 Sites

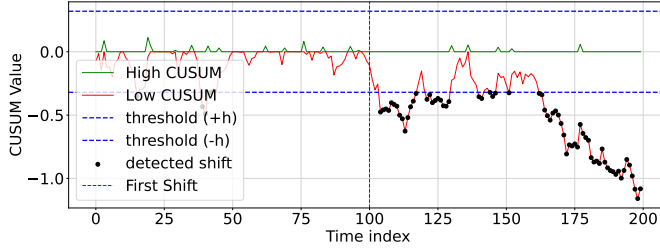
We found information of sites only within the RSNA dataset (presented in Table 1). The performance metrics based on the two sites are presented in Fig. 2i. We observe that for RSNA, site 2 outperforms site 1 in PPV by 24.4%, in sensitivity by 14.45% and in AUROC by 3% ( $p < 0.03$ ) despite having more training samples (with higher prevalence) from site 1 than site 2.

In addition to the individual attribute analysis, we also conducted a joint attribute analysis, including age-race, race-density, and age-density for EMBED, as presented in Appendix C.1. The findings from this analysis are consistent with those discussed in this section.

From the preceding analysis, the model for EMBED achieves good PPV (> 88%) for almost all subgroups except for the ‘70 ≤ age < 80’ group and the AAB group. The model also achieves a good sensitivity for almost all subgroups ranging from 66.70% to 74.17%, except the drops for the Caucasian population with age ≥ 80, the AAB population with tissue density of 1, NHPI race, and MLO view groups. The model for RSNA achieves reasonable performance for all subgroups, except a lower PPV for the ‘40 ≤ age < 50’ group, and lower sensitivity for the density of 4 group. High AUROC is achieved for most subgroups for both datasets except the drops for ‘age < 40’ group in the EMBED-AI model and for the ‘40 ≤ age < 50’ and ‘70 ≤ age < 80’ groups in RSNA-AI model. The lower performing groups may benefit from alternative or supplemental screening. For most cases in both datasets, no significant difference is found among the performance metrics of different scanners. High specificity (≥ 98.44% from Table C4 - C5) indicates low false positive rates for



(a)



(b)

**Fig. 3:** CUSUM based sensitivity monitoring charts. The batches are assumed to form a sequential data. After time index 100, we add more samples from the underperforming (a) the NHPI and (b) ‘age  $\geq 80$ ’ groups of EMBED to each batch to introduce performance drift.

all subgroups. Model uncertainty demonstrates only a nominal variation, remaining within a narrow range across the subgroups. Moreover, we observe that the EMBED-AI model demonstrates lower variability in performance across subgroups compared to the RSNA model.

To investigate how much additional performance deviation is introduced by the training algorithm or the model, we present the statistical association between the targets (or predicted labels) and the attributes in Table 3. The associations between targets and attributes represent the underlying relationships of data, and the associations between attributes and model predictions represent how much of the relationship is mirrored by the model. From the Table we observe that there is a significant association present only between the age groups and targets for both datasets. The model mirrors the relationships significantly well for most attributes except that there is a slight drop in association between age groups and predicted labels.

### 3.3 Monitoring Performance Drift

Here, we show how CUSUM can be used to monitor drift in model performance. Specifically, we monitor the sensitivity. The number of bootstrapped batches  $N$  is set to 200 and the batch size  $B$  is 1000. The number of positive samples for a subgroup

within a batch is set equal to the base prevalence ratio from the data distribution. We assume that the first 100 batches are formed from the base empirical distribution and the rest of the batches come from the shifted distribution.

To present a specific case, after batch 100, we start adding more samples to each batch from the underperforming NHPI and ‘age  $\geq 80$ ’ subgroups of EMBED at a fixed  $\Delta p$  of 0.3 to introduce a drift in sensitivity, which we aim to detect.  $k$  is tuned from  $\{0.0, 0.01, 0.02, \dots, 0.1\}$ . We present the drift detection charts in Fig. 3. FAR and drift detection delays are presented in Table C6 in Appendix C.2. There are only a few false alarms with a minimal average detection delay. The few initial false positives in Fig. 3 indicate a temporary drop in sensitivity. Then, the control signal goes up again within the threshold range. However, the detected sharp drift after index 100 indicates a permanent degradation in sensitivity below the acceptable range and follow up adjustments to the model is necessary. Therefore, the CUSUM based monitoring method is effective in quickly detecting permanent performance drifts.

Next, we simulate CUSUM monitoring by varying the deviating subgroup  $u$  and the deviation  $\Delta p$  to monitor the effects of these shifts in data distribution. The lower control value at the end of a certain simulation  $S^l(N)$  represents the relative quantity of performance drop for the introduced deviation at the simulation. We present these relative sensitivity drops in Fig. 4. We observe from Fig. 4a that for EMBED, compared to the performance of base distribution (when  $\Delta p = 0$ ), sensitivity drops rapidly even when there is a slight increase of samples from the ‘age  $\geq 80$ ’ group. However, for the ‘ $60 \leq \text{age} < 70$ ’ group, the sensitivity drops slowly with large deviations. Similarly, in Fig. 4b, we observe that sensitivity drops at different rates with increasing deviations for the AIAN and the NHPI group. On the contrary in Fig. 4c, although we observe sensitivity drops for large deviations in certain age groups, the drops are small for the RSNA dataset compared to the baseline performance.

Monitoring performance drift with CUSUM is important, as it enables the early detection of performance degradation when new data are introduced, particularly when demographic shifts lead to underperformance. By identifying these changes in real time, CUSUM ensures that model performance remains accurate, equitable, and reliable, helping to prevent bias and ensuring fair treatment across diverse patient populations. This proactive monitoring not only helps sustain the effectiveness of predictive models during deployment but also mitigates the risk of worsening outcomes for underrepresented subgroups.

## 4 Related Work

Since the introduction of deep learning, computer aided diagnosis received a great deal of attention in the research community. BCD models for digital mammography can ease the screening process for practitioners and reduce mortality. Researchers explored various deep architectures and methodologies to train BCD models. Sahu et al. (2023); Raiaan et al. (2024); Qureshi et al. (2024); Mahoro and Akhloufi (2022); Petrini et al. (2022); Wang et al. (2023); Altameem et al. (2022); Shen et al. (2019) train BCD models on different datasets. However, these models are of limited capacity as they are trained on smaller datasets with degraded resolutions and only a few positive cases.

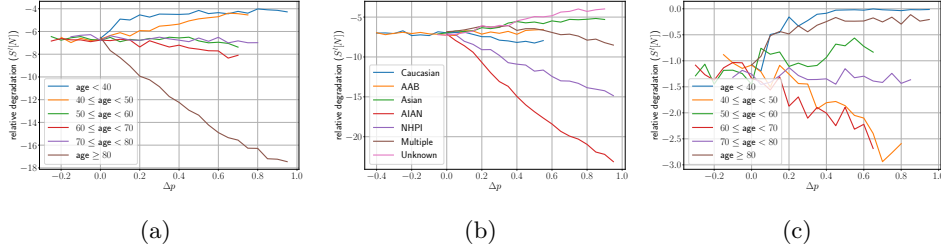


**Fig. 4:** Monitoring sensitivity drops under the distribution shifts of subgroups, such as by deviating the proportion of (a) age groups from EMBED, (b) racial groups from EMBED and (c) age groups from RSNA. Here,  $k$  is set to 0.

For example, the datasets such as Mini-DDSM by [Lekamlage et al. \(2020\)](#); [Heath et al. \(1998\)](#), CMMD by [Cui et al. \(2021\)](#), CDD-CESM by [Khaled et al. \(2021\)](#), BMCD by [Loizidou et al. \(2021\)](#) have less than 10000 mammograms, while VinDr-Mammo by [Pham et al. \(2022\)](#) has 20000 mammograms. OMI-DB by [Halling-Brown et al. \(2020\)](#) is a large dataset in mammography. However, these datasets lack sufficient patient demographic and other clinical information, which raises concerns about the possibility of bias in the previous models.

In this regard, EMBED by [Jeong et al. \(2023\)](#) and RSNA ([Carr et al. \(2022\)](#)) are large datasets that include rich information about demographics, and clinical attributes. We find only a few works in the literature that utilized these datasets for developing BCD AI models. [Khara et al. \(2024\)](#) train ResNets for tissue density and race classification, while [Donnelly et al. \(2024\)](#) develop a 1 to 5 year cancer risk prediction model on EMBED. [Correa et al. \(2024\)](#) designed an adversarial debiasing approach with partial learning to reduce racial disparities for the density classification task. [Hwang et al. \(2023\)](#) train ResNet models for BCD with only 1441 samples from EMBED and the other datasets and assessed AUROC across the racial groups. [Zhang et al. \(2023\)](#) develop abnormal lesion classification models and analyze the performance across subgroups based on demography, pathology outcomes and image findings. These works select a balanced dataset for training, which does not reflect the real scenario. Therefore, there is a need for a BCD model trained on a large and diverse dataset and for analyzing the model across the most important subgroups.

[Sun et al. \(2022\)](#) demonstrate a comprehensive performance analysis on the COVID-19 detection model from chest X-rays. [Afzal et al. \(2023\)](#) perform a comprehensive analysis for kidney tumor segmentation across the demographic groups. [Mehta et al. \(2024\)](#) analyze the uncertainty in model performance among the subgroups for three medical applications. Following this, we aim to analyze our BCD AI model performance across the relevant subgroups. Recently, [Nguyen et al. \(2024\)](#) studies the false positive rates across different demographic groups on a commercial AI model for the DBT examinations. However, it is hard to understand the significance of these results since no details are provided about the training data.

[Vela et al. \(2022\)](#) demonstrates that the quality of AI model may drop over time for various applications. For BCD-AI models, the performance of the model may drop

due to shifts in the distribution of demographics, scanning technology, and local processes (Sahiner et al. (2023)). In this regard, Nestor et al. (2019) demonstrates that the performance of the model trained on electronic health records degrades due to distribution changes. To monitor the performance over time, Prathapan et al. (2024); Zamzmi et al. (2024) adopt methods from statistical process control either using simulated mean shifts in performance or by inserting out of distribution data. However, in our paper, we monitor the model performance due to shifts in patient demographics.

## 5 Conclusion

We develop a high-performing AI model on EMBED using advanced computer vision training strategies using limited computational resources. Despite training the models on diverse datasets that incorporate demographic and clinical information and achieving overall good performance, we identify a few significant cases of performance disparities. For EMBED, we observe lower PPV for the ‘ $70 \leq \text{age} < 80$ ’ and African American groups, and lower sensitivity for the Caucasian population with ‘ $\text{age} \geq 80$ ’, the African American population with tissue density 1, NHPI population and MLO view groups. For RSNA, we observe reasonably good performance for all subgroups, except a lower PPV for the ‘ $40 \leq \text{age} < 50$ ’ group, and lower sensitivity for the density of 4 group. Unreliable sensitivity estimates of AIAN and NHPI population due to low number of samples emphasizes the need to collect more data for these populations to ensure fairness for all patients. Existing data balancing or targeted fairness-driven retraining techniques may not significantly improve the sensitivity estimates due low number of positive test samples for these groups. Our analysis reveals that our EMBED model exhibits lower performance variability across subgroups compared to the RSNA model. With this subgroup analysis framework, we can identify the biases inherited in the training data and show that biases in the data could lead to potential disparities in clinical outcomes for some groups even with well-trained AI models. Care should be taken while deploying such models by monitoring the performance of such underperforming subgroups. Finally, we show that CUSUM based charts can effectively monitor the model performance over time as local populations shift (e.g. new age demographics, variations in scanners, or locations), where it can quickly flag the performance drop, enabling appropriate interventions, such as model retraining or recalibration. The results from the comprehensive analysis can inform the development of evaluation techniques for unbiased breast cancer detection models from digital mammography.

Implementing a monitoring system that flags performance drops for underrepresented groups can have several clinical implications. One of the key benefits is the timely identification of performance disparities. CUSUM allows for real-time monitoring and quickly detecting when a model’s accuracy diminishes for specific demographics, such as certain age groups, racial or ethnic communities. Early identification of these disparities enables clinicians to take action, ensuring that underserved groups are not left at the disadvantage of a lower prediction of BCD. Further, as local populations evolve, whether through demographic shifts or changes in healthcare infrastructure (e.g., variations in scanner types or staff training), the performance of BCD models can also fluctuate. A continuous monitoring method helps address these

changes by quickly flagging any decline in model performance due to these factors. When such a performance drop is detected, it can prompt timely interventions like model retraining with updated, representative data or recalibration to restore performance. This dynamic approach ensures that models remain effective as healthcare conditions evolve. This real-time monitoring can also enable proactive clinical interventions. For example, if a performance issue is flagged for an underrepresented group, healthcare providers can adjust the model’s parameters or incorporate additional training data to improve predictions. Such interventions enhance the model’s ability to detect breast cancer more accurately across all patient groups, especially in communities that may have historically faced challenges with underdiagnosis or misdiagnosis. This proactive approach ensures that the model continues to serve all populations effectively, potentially reducing health disparities in breast cancer detection.

In the long-term, the use of continuous monitoring can contribute to a more equitable healthcare system. By continuously refining models based on real-world performance data, biases can be identified and corrected early, preventing the reinforcement of healthcare disparities. This creates a cycle of continuous improvement, where BCD models evolve to become more inclusive and accurate for all populations, ensuring that advancements in technology benefit everyone, regardless of demographic factors.

#### **Author Contribution.**

#### **Funding.**

**Data Availability.** The datasets used in this research are found publicly available at [Carr et al. \(2022\)](#) and [Jeong et al. \(2023\)](#).

**Acknowledgments.** We are grateful of the support and resources provided by the University of Maryland Institute for Health Computing and for the IT support provided by Jonathan Heagerty throughout the project.

## **Declarations**

**Ethical Approval.** This research does not require Institutional Review Board approval.

**Conflict of Interest.** The authors declare no competing interests.

## **References**

- Afzal, M.M., Khan, M.O., Mirza, S.: Towards equitable kidney tumor segmentation: Bias evaluation and mitigation. In: Machine Learning for Health (ML4H), pp. 13–26 (2023). PMLR
- Altameem, A., Mahanty, C., Poonia, R.C., Saudagar, A.K.J., Kumar, R.: Breast cancer detection in mammography images using deep convolutional neural networks and fuzzy ensemble modeling techniques. *Diagnostics* **12**(8), 1812 (2022)

- Azin, A., Tahmasebi, H., Brar, A., Azin, S., Ko, G., Covelli, A., Cil, T.: Racial, ethnic and socioeconomic disparities in diagnosis, treatment, and survival of patients with breast cancer. *The American Journal of Surgery* **225**(1), 154–161 (2023)
- Carr, C., Kitamura, F., Partridge, G., Kalpathy-Cramer, J., Mongan, J., Andriole, K., Maryam Vazirabad, M.R., Ball, R., Dane, S., Chen, Y.: RSNA Screening Mammography Breast Cancer Detection. Kaggle (2022). <https://kaggle.com/competitions/rsna-breast-cancer-detection>
- Cui, C., Li, L., Cai, H., Fan, Z., Zhang, L., Dan, T., Li, J., Wang, J.: The Chinese Mammography Database (CMMD): An online mammography database with biopsy confirmed types for machine diagnosis of breast (2021)
- Coleman, C.: Early detection and screening for breast cancer. In: *Seminars in Oncology Nursing*, vol. 33, pp. 141–155 (2017). Elsevier
- Correa, R., Pahwa, K., Patel, B., Vachon, C.M., Gichoya, J.W., Banerjee, I.: Efficient adversarial debiasing with concept activation vector—medical image case-studies. *Journal of Biomedical Informatics* **149**, 104548 (2024)
- Crosier, R.B.: A new two-sided cumulative sum quality control scheme. *Technometrics* **28**(3), 187–194 (1986)
- Donnelly, J., Moffett, L., Barnett, A.J., Trivedi, H., Schwartz, F., Lo, J., Rudin, C.: AsymMirai: Interpretable mammography-based deep learning model for 1–5-year breast cancer risk prediction. *Radiology* **310**(3), 232780 (2024)
- Dunn, O.J.: Multiple comparisons using rank sums. *Technometrics* **6**(3), 241–252 (1964)
- De Vries, T., Misra, I., Wang, C., Maaten, L.: Does object recognition work for everyone? In: *Proceedings of the IEEE/CVF Conference on Computer Vision and Pattern Recognition Workshops*, pp. 52–59 (2019)
- Evans, K.K., Birdwell, R.L., Wolfe, J.M.: If you don’t find it often, you often don’t find it: why some cancers are missed in breast cancer screening. *PloS one* **8**(5), 64366 (2013)
- Feng, J., Phillips, R.V., Malenica, I., Bishara, A., Hubbard, A.E., Celi, L.A., Pirracchio, R.: Clinical artificial intelligence quality improvement: towards continual monitoring and updating of AI algorithms in healthcare. *NPJ Digital Medicine* **5**(1), 66 (2022)
- Ge, Z.: YOLOX: Exceeding YOLO series in 2021. arXiv preprint arXiv:2107.08430 (2021)
- Gal, Y., Ghahramani, Z.: Dropout as a bayesian approximation: Representing model

- uncertainty in deep learning. In: International Conference on Machine Learning, pp. 1050–1059 (2016). PMLR
- Ginsburg, O., Yip, C.-H., Brooks, A., Cabanes, A., Caleffi, M., Dunstan Yataco, J.A., Gyawali, B., McCormack, V., Anderson, M., Mehrotra, R., *et al.*: Breast cancer early detection: A phased approach to implementation. *Cancer* **126**, 2379–2393 (2020)
- Heath, M., Bowyer, K., Kopans, D., Kegelmeyer Jr, P., Moore, R., Chang, K., Munishkumaran, S.: Current status of the digital database for screening mammography. In: *Digital Mammography: Nijmegen, 1998*, pp. 457–460. Springer, ??? (1998)
- Halling-Brown, M.D., Warren, L.M., Ward, D., Lewis, E., Mackenzie, A., Wallis, M.G., Wilkinson, L.S., Given-Wilson, R.M., McAvinchey, R., Young, K.C.: Optima mam mammography image database: a large-scale resource of mammography images and clinical data. *Radiology: Artificial Intelligence* **3**(1), 200103 (2020)
- Hussain-Gambles, M., Atkin, K., Leese, B.: Why ethnic minority groups are under-represented in clinical trials: a review of the literature. *Health & Social Care in the Community* **12**(5), 382–388 (2004)
- Hershman, D., McBride, R., Jacobson, J.S., Lamerato, L., Roberts, K., Grann, V.R., Neugut, A.I.: Racial disparities in treatment and survival among women with early-stage breast cancer. *Journal of Clinical Oncology* **23**(27), 6639–6646 (2005)
- Huang, G., Sun, Y., Liu, Z., Sedra, D., Weinberger, K.Q.: Deep networks with stochastic depth. In: *Computer Vision–ECCV 2016: 14th European Conference, Amsterdam, The Netherlands, October 11–14, 2016, Proceedings, Part IV 14*, pp. 646–661 (2016). Springer
- Hwang, I.C., Trivedi, H., Brown-Mulry, B., Zhang, L., Nalla, V., Gastounioti, A., Gichoya, J., Seyyed-Kalantari, L., Banerjee, I., Woo, M.: Impact of multi-source data augmentation on performance of convolutional neural networks for abnormality classification in mammography. *Frontiers in Radiology* **3**, 1181190 (2023)
- Jeong, J.J., Vey, B.L., Bhimoreddy, A., Kim, T., Santos, T., Correa, R., Dutt, R., Mosunjac, M., Oprea-Ilies, G., Smith, G., *et al.*: The emory breast imaging dataset (EMBED): A racially diverse, granular dataset of 3.4 million screening and diagnostic mammographic images. *Radiology: Artificial Intelligence* **5**(1), 220047 (2023)
- Khaled, R., Helal, M., Alfarghaly, O., Mokhtar, O., Elkorany, A., El Kassas, H., Fahmy, A.: Categorized Digital Database for Low energy and Subtracted Contrast Enhanced Spectral Mammography images [Dataset]. The Cancer Imaging Archive (2021). <https://doi.org/10.7937/29kw-ae92>
- Khara, G., Trivedi, H., Newell, M.S., Patel, R., Rijken, T., Kecskemethy, P., Glocker, B.: Generalisable deep learning method for mammographic density prediction across

- imaging techniques and self-reported race. *Communications Medicine* **4**(1), 21 (2024)
- Kruskal, W.H., Wallis, W.A.: Use of ranks in one-criterion variance analysis. *Journal of the American statistical Association* **47**(260), 583–621 (1952)
- Lekamlage, C.D., Afzal, F., Westerberg, E., Cheddad, A.: Mini-ddsm: Mammography-based automatic age estimation. In: *Proceedings of the 3rd International Conference on Digital Medicine and Image Processing*, pp. 1–6 (2020)
- Lukasik, M., Bhojanapalli, S., Menon, A., Kumar, S.: Does label smoothing mitigate label noise? In: *International Conference on Machine Learning*, pp. 6448–6458 (2020). PMLR
- Loshchilov, I., Hutter, F.: Sgdr: Stochastic gradient descent with warm restarts. *arXiv preprint arXiv:1608.03983* (2016)
- Liu, Z., Mao, H., Wu, C.-Y., Feichtenhofer, C., Darrell, T., Xie, S.: A convnet for the 2020s. In: *Proceedings of the IEEE/CVF Conference on Computer Vision and Pattern Recognition*, pp. 11976–11986 (2022)
- Loizidou, K., Skouroumouni, G., Pitris, C., Nikolaou, C.: Digital subtraction of temporally sequential mammograms for improved detection and classification of microcalcifications. *European Radiology Experimental* **5**, 1–12 (2021)
- Mahoro, E., Akhloufi, M.A.: Applying deep learning for breast cancer detection in radiology. *Current Oncology* **29**(11), 8767–8793 (2022)
- Maxwell, A.J.: Breast cancers missed in the prevalent screening round: effect upon the size distribution of incident round detected cancers. *Journal of Medical Screening* **6**(1), 28–29 (1999)
- Morales-Brotons, D., Vogels, T., Hendrikx, H.: Exponential moving average of weights in deep learning: Dynamics and benefits. *Transactions on Machine Learning Research* (2024)
- Mehta, R., Shui, C., Arbel, T.: Evaluating the fairness of deep learning uncertainty estimates in medical image analysis. In: *Medical Imaging with Deep Learning*, pp. 1453–1492 (2024). PMLR
- Mann, H.B., Whitney, D.R.: On a test of whether one of two random variables is stochastically larger than the other. *The annals of mathematical statistics*, 50–60 (1947)
- Nguyen, H.D.: Kaggle RSNA Breast Cancer Detection. [https://github.com/dangnh0611/kaggle\\_rsna\\_breast\\_cancer](https://github.com/dangnh0611/kaggle_rsna_breast_cancer). Accessed on August 15, 2024 (2023)
- Newman, L.A., Kaljee, L.M.: Health disparities and triple-negative breast cancer in

- african american women: a review. *JAMA surgery* **152**(5), 485–493 (2017)
- Nestor, B., McDermott, M.B., Boag, W., Berner, G., Naumann, T., Hughes, M.C., Goldenberg, A., Ghassemi, M.: Feature robustness in non-stationary health records: caveats to deployable model performance in common clinical machine learning tasks. In: *Machine Learning for Healthcare Conference*, pp. 381–405 (2019). PMLR
- Nguyen, D.L., Ren, Y., Jones, T.M., Thomas, S.M., Lo, J.Y., Grimm, L.J.: Patient characteristics impact performance of ai algorithm in interpreting negative screening digital breast tomosynthesis studies. *Radiology* **311**(2), 232286 (2024)
- Nicholson, W.K., Silverstein, M., Wong, J.B., Barry, M.J., Chelmow, D., Coker, T.R., Davis, E.M., Jaén, C.R., Krousel-Wood, M., Lee, S., et al.: Screening for breast cancer: Us preventive services task force recommendation statement. *JAMA* (2024)
- Obermeyer, Z., Powers, B., Vogeli, C., Mullainathan, S.: Dissecting racial bias in an algorithm used to manage the health of populations. *Science* **366**(6464), 447–453 (2019)
- Prathapan, S., Samala, R.K., Hadjiyski, N., D’Haese, P.-F., Maldonado, F., Nguyen, P., Yesha, Y., Sahiner, B.: Quantifying input data drift in medical machine learning models by detecting change-points in time-series data. In: *Medical Imaging 2024: Computer-Aided Diagnosis*, vol. 12927, pp. 67–76 (2024). SPIE
- Petrini, D.G., Shimizu, C., Roela, R.A., Valente, G.V., Folgueira, M.A.A.K., Kim, H.Y.: Breast cancer diagnosis in two-view mammography using end-to-end trained efficientnet-based convolutional network. *IEEE ACCESS* **10**, 77723–77731 (2022)
- Pham, H.H., Trung, H.N., Nguyen, H.Q.: Vindr-mammo: A large-scale benchmark dataset for computer-aided detection and diagnosis in full-field digital mammography. *Sci Data* (2022)
- Qureshi, S.A., Hussain, L., Shah, S.T.H., Mir, A.A., Williams, D.K.A., Duong, T.Q., Habib, N., Ahmad, A., Shah, S.A.H., et al.: Breast cancer detection using mammography: Image processing to deep learning (2024)
- Raiaan, M.A.K., Fahad, N.M., Mukta, M.S.H., Shatabda, S.: Mammo-light: A lightweight convolutional neural network for diagnosing breast cancer from mammography images. *Biomedical Signal Processing and Control* **94**, 106279 (2024)
- Sahiner, B., Chen, W., Samala, R.K., Petrick, N.: Data drift in medical machine learning: implications and potential remedies. *The British Journal of Radiology* **96**(1150), 20220878 (2023)
- Sahu, A., Das, P.K., Meher, S.: Recent advancements in machine learning and deep learning-based breast cancer detection using mammograms. *Physica Medica* **114**, 103138 (2023)

- Sweeney, C., Ennis, E., Mulvenna, M., Bond, R., O'Neill, S.: How machine learning classification accuracy changes in a happiness dataset with different demographic groups. *Computers* **11**(5), 83 (2022)
- Sickles, E.A.: ACR BI-RADS atlas, breast imaging reporting and data system. *American College of Radiology*, 39 (2013)
- Shen, L., Margolies, L.R., Rothstein, J.H., Fluder, E., McBride, R., Sieh, W.: Deep learning to improve breast cancer detection on screening mammography. *Scientific reports* **9**(1), 12495 (2019)
- Sun, J., Peng, L., Li, T., Adila, D., Zaiman, Z., Melton-Meaux, G.B., Ingraham, N.E., Murray, E., Boley, D., Switzer, S., *et al.*: Performance of a chest radiograph ai diagnostic tool for covid-19: A prospective observational study. *Radiology: Artificial Intelligence* **4**(4), 210217 (2022)
- Vela, D., Sharp, A., Zhang, R., Nguyen, T., Hoang, A., Pianykh, O.S.: Temporal quality degradation in ai models. *Scientific Reports* **12**(1), 11654 (2022)
- Wilson, B., Hoffman, J., Morgenstern, J.: Predictive inequity in object detection. *arXiv preprint arXiv:1902.11097* (2019)
- Wang, K., Tikhonov, A., Hill, M., Litchfield, L.: Evaluating mammogram image classification: Impact of model architectures, pretraining, and finetuning. In: *Pacific-Rim Symposium on Image and Video Technology*, pp. 1–14 (2023). Springer
- Yedjou, C.G., Sims, J.N., Miele, L., Noubissi, F., Lowe, L., Fonseca, D.D., Alo, R.A., Payton, M., Tchounwou, P.B.: Health and racial disparity in breast cancer. *Breast Cancer Metastasis and Drug Resistance: Challenges and Progress*, 31–49 (2019)
- Zhang, L., Brown-Mulry, B., Nalla, V., Hwang, I.C., Gichoya, J.W., Gastounioti, A., Banerjee, I., Seyyed-Kalantari, L., Woo, M., Trivedi, H.: Multivariate analysis on performance gaps of artificial intelligence models in screening mammography. *arXiv preprint arXiv:2305.04422* (2023)
- Zamzmi, G., Venkatesh, K., Nelson, B., Prathapan, S., Yi, P.H., Sahiner, B., Delfino, J.G.: Out-of-distribution detection and data drift monitoring using statistical process control. *arXiv preprint arXiv:2402.08088* (2024)

## Appendix A BIRADS Definitions

We provide the definitions of different BIRADS scores in Table A2 and tissue densities in Table A1. Some mammogram examples based on the BIRADS scores are presented in Fig. A1.

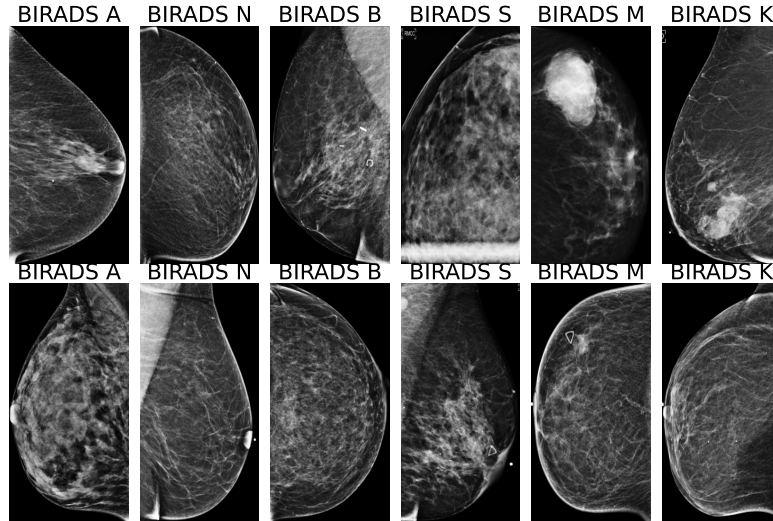


Fig. A1: Sample mammograms for different BIRADS scores

Table A1: Definition of BIRADS tissue densities

Density	BIRADS	Tissue description
1	A	fatty tissue
2	B	scattered fibroglandular
3	C	heterogeneously dense
4	D	extremely dense
5	–	male tissue

Table A2: Definition of BIRADS scores for mammogram screening

scores	0 or A	1 or N	2 or B	3 or P	4 or S	5 or M	6 or K
Findings	additional evaluation required	normal tissue	benign findings	probably benign	suspicious	highly suspicious	proven malignancy

## Appendix B Training Details

Here we present the preprocessing details of each mammogram, the set of input augmentations and the choice of hyperparameters for training the model.

**Table B3:** Correlation or Association ( $p < 0.05$ ) between variables within the datasets

	EMBED			
group	age	race	density	view
race	0.0904			
density	-0.21 <sup>4</sup>	0.1199		
view	0.0092	0.0069 <sup>3</sup>	0.008	
machine	0.02449	0.0538	0.0509	0.0063 <sup>3</sup>
	RSNA			
group	age	site	density	view
site	0.2976			
density	-0.258 <sup>4</sup>			
view	0.0125 <sup>3</sup>	0.0087	0.0292	
machine	0.1426	1	0.0652	0.0163 <sup>3</sup>

<sup>3</sup>indicates where correlation or association is not significant ( $p > 0.05$ )

<sup>4</sup>instead of considering as categorical variables, here the spearman correlation coefficient is measured between age and density.

### B.1 Preprocessing

For each mammogram, we first read the DICOM meta data, convert it to 8 bit integers, and normalize them between 0 to 255. Next, an off-the-shelf YOLOX-nano  $416 \times 416$  model (Ge (2021)) is applied as the ROI extractor that crops the breast area to retrain the texture of the mammogram. Finally, the image is resized to  $1024 \times 2048$  to be utilized as the input to the model. This preprocessing step removes the unnecessary dark background from the input.

### B.2 Augmentations

We apply a specific set of augmentations to the inputs following Nguyen (2023). During training, we apply random cropping, changes in brightness or contrast, down scaling, geometric distortions such as shifts, rotation, elastic transformations, grid distortions, and random erasures with certain probabilities. We also randomly apply horizontal and vertical flipping with probability of 0.5. We normalize the images with the ImageNet dataset mean and standard deviation.

### B.3 Hyperparameters

We train the model with a batch size of 8 for 15 epochs. We use a SGD optimizer with a learning rate of 0.001, momentum of 0.9, weight decay of  $2 \times 10^{-6}$  and a cosine

annealed scheduling. An exponential moving average (EMA) model is tracked with a decay of 0.9998, and used for final evaluation. A binary cross-entropy loss is employed with smoothing only for the positive samples using a smoothing parameter of 0.2. We use a balanced batch sampling with positive to negative sample ratio at 1 : 1. We train the small ConvNext model with dropout at a rate of 0.5 and a drop path rate of 0.2.

## B.4 Model Uncertainty Estimation

Model uncertainty is measured using the Monte Carlo (MC) dropout method by Gal and Ghahramani (2016). Since our model is trained with dropout, this method involves activating dropout during inference. The model is run multiple times with different dropout masks, generating a distribution of predictions for the same sample. The uncertainty is then defined as the standard deviation of these predictions.

# Appendix C Additional Results

## C.1 Detailed results based on the attributes

The detailed results on EMBED and RSNA with the range of classification metrics for different subgroups are presented in Table C4 and Table C5 respectively. We also present the subgroup analysis based on the joint attributes, such as age-race, race-density and age-density for EMBED in Fig. C2.

## C.2 Performance Monitoring

The tuned  $k$  value, the number of false positives, and detection delays are presented in Table C6. We can observe that there are only a few false positives with only a minimal average detection delay.

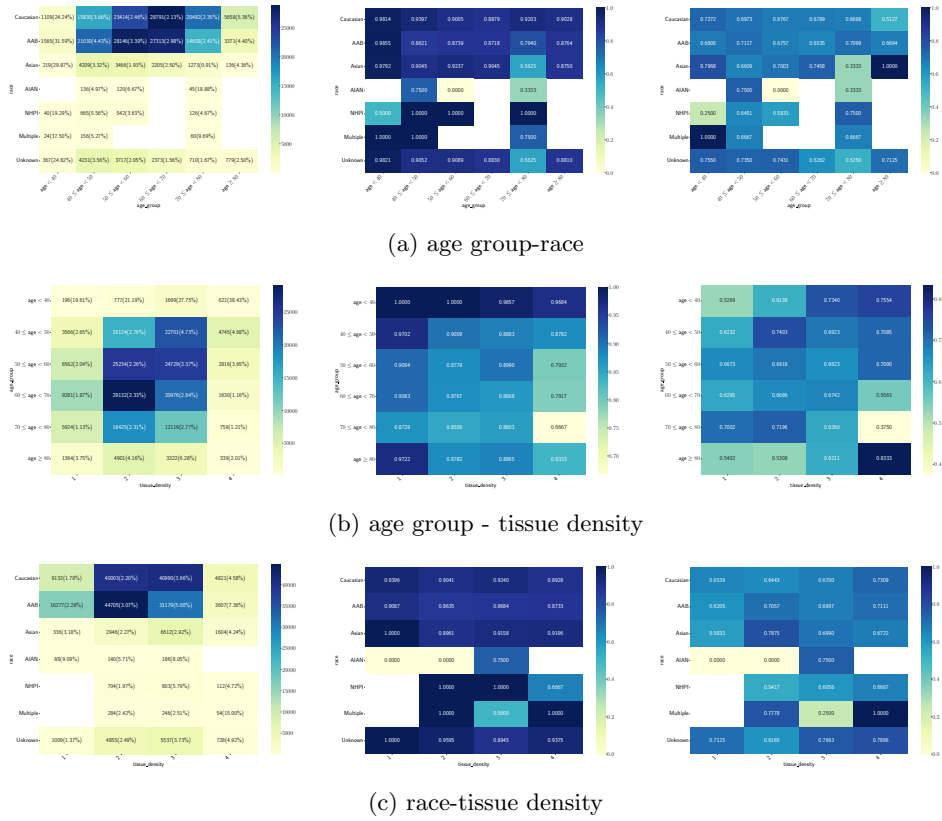


**Fig. C2:** The number of samples, PPV, and sensitivity for the joint attribute based subgroups in EMBED, such as (a) age group-race, (b) age group-tissue density and (c) race-tissue density. The blank cells indicate no positive test samples for these groups.

**Table C4:** Detailed subgroup results on the EMBED dataset

Groups	AU-ROC	PPV	sensitivity	F1 score	specificity	accuracy	uncertainty
age < 40	0.9287	0.9827	0.7099	0.8238	0.9951	0.9146	0.0682
40 ≤ age < 50	0.9347	0.8958	0.7038	0.7882	0.9966	0.9849	0.0656
50 ≤ age < 60	0.9500	0.8870	0.6776	0.7679	0.9975	0.9884	0.0597
60 ≤ age < 70	0.9420	0.8803	0.6670	0.7587	0.9977	0.9895	0.06
70 ≤ age < 80	0.9513	0.8573	0.6773	0.7566	0.9973	0.9898	0.0657
age ≥ 80	0.9482	0.8904	0.5741	0.6975	0.9964	0.9761	0.0763
Caucasian	0.9484	0.9173	0.6676	0.7726	0.9982	0.9884	0.0618
AAB	0.9407	0.8747	0.6831	0.7670	0.9961	0.9841	0.0643
Asian	0.9395	0.9136	0.7038	0.7940	0.9979	0.9890	0.0639
AIAN	0.9236	1.0	0.7083	0.8167	1.0	0.9839	0.0591
NHPI	0.9259	1.0	0.6019	0.7470	1.0	0.9850	0.0628
Multiple	0.9866	0.9167	0.7417	0.7889	0.9983	0.9910	0.0625
Unknown	0.9552	0.9207	0.7139	0.8030	0.9980	0.9889	0.0605
density 1	0.9578	0.9372	0.6492	0.7670	0.9988	0.9897	0.0514
density 2	0.9463	0.8829	0.6798	0.7680	0.9976	0.9892	0.0585
density 3	0.9355	0.8976	0.6771	0.7717	0.9967	0.9835	0.0694
density 4	0.9479	0.8914	0.7210	0.7962	0.9949	0.9799	0.0788
MLO view	0.9393	0.8881	0.6428	0.7455	0.9977	0.9881	0.0616
CC view	0.9481	0.9014	0.7063	0.7918	0.9967	0.9847	0.0645
Lorad Selenia	0.9499	0.8346	0.7567	0.7923	0.9964	0.9906	0.0627
Selenia Dimensions	0.9446	0.8985	0.6814	0.7749	0.9972	0.9863	0.0659
S2000D ADS17.4.5	0.9530	0.9038	0.6479	0.7534	0.9976	0.9872	0.06
S2000D ADS17.5	0.9349	0.9008	0.6181	0.7187	0.9974	0.9861	0.0679
SEss. ADS53.40	0.9413	0.8751	0.6277	0.7222	0.9978	0.9889	0.0625
S Pristina	0.9358	0.75	0.2604	0.3745	1.0	0.9647	0.0656

**Table C5:** Detailed subgroup results on the RSNA dataset

Groups	AUROC	PPV	sensi- tivity	F1 score	speci- ficity	accuracy	uncer- tainty
age < 40	0.9994	0.8452	0.90	0.8504	0.9979	0.9968	0.0086
40 ≤ age < 50	0.9110	0.4442	0.5111	0.4748	0.9942	0.9898	0.0104
50 ≤ age < 60	0.9330	0.54	0.5489	0.5437	0.9928	0.9861	0.0115
60 ≤ age < 70	0.9303	0.5735	0.5126	0.5405	0.9908	0.9797	0.0138
70 ≤ age < 80	0.9076	0.7050	0.5261	0.6026	0.9888	0.9665	0.0199
age ≥ 80	0.9352	0.5750	0.5819	0.5777	0.9770	0.9574	0.0264
site 1	0.9164	0.4854	0.4684	0.4761	0.9884	0.9767	0.0155
site 2	0.9463	0.7294	0.6129	0.6658	0.9954	0.9879	0.0106
density 1	0.9075	0.4595	0.50	0.4771	0.9895	0.9812	0.0127
density 2	0.9101	0.4620	0.4830	0.4714	0.9857	0.9734	0.0169
density 3	0.9203	0.5162	0.4504	0.4806	0.9901	0.9778	0.0156
density 4	0.9529	0.6062	0.42	0.4938	0.9954	0.9860	0.0113
MLO view	0.9312	0.5747	0.5127	0.5412	0.9917	0.9816	0.0140
CC view	0.9328	0.5892	0.5499	0.5686	0.9917	0.9823	0.0126
machine 21	0.9532	0.7857	0.5909	0.6724	0.9967	0.9891	0.0082
machine 29	0.9377	0.7061	0.5901	0.6413	0.9951	0.9872	0.0119
machine 48	0.9513	0.7143	0.6522	0.6817	0.9945	0.9875	0.0116
machine 49	0.9107	0.5147	0.4646	0.4876	0.9881	0.9744	0.0163
machine 93	0.9637	0.2933	0.6071	0.3953	0.9891	0.9863	0.0117
machine 170	0.9398	0.5042	0.6196	0.5554	0.9844	0.9754	0.0182
machine 190	0.8661	0.6405	0.50	0.5304	0.9875	0.9707	0.0180

**Table C6:** Sensitivity monitoring results with design choices

under-performing group	Tuned $k$	FAR	Detection Delay
NHPI	0.06	1	1
'age ≥ 80'	0.06	4	2